



Stodieck, O., Cooper, J. E., Weaver, P. M., & Kealy, P. (2015). Optimization of Tow-Steered Composite Wing Laminates for Aeroelastic Tailoring. *AIAA Journal*, 53(8), 2203-2215. 10.2514/1.J053599

Peer reviewed version

Link to published version (if available):
[10.2514/1.J053599](https://doi.org/10.2514/1.J053599)

[Link to publication record in Explore Bristol Research](#)
PDF-document

University of Bristol - Explore Bristol Research

General rights

This document is made available in accordance with publisher policies. Please cite only the published version using the reference above. Full terms of use are available:
<http://www.bristol.ac.uk/pure/about/ebr-terms.html>

Take down policy

Explore Bristol Research is a digital archive and the intention is that deposited content should not be removed. However, if you believe that this version of the work breaches copyright law please contact open-access@bristol.ac.uk and include the following information in your message:

- Your contact details
- Bibliographic details for the item, including a URL
- An outline of the nature of the complaint

On receipt of your message the Open Access Team will immediately investigate your claim, make an initial judgement of the validity of the claim and, where appropriate, withdraw the item in question from public view.

Optimization of Tow-Steered Composite Wing Laminates for Aeroelastic Tailoring

O. Stodieck¹, J. E. Cooper², P. M. Weaver³

Department of Aerospace Engineering, University of Bristol, Bristol BS8 1TR, U.K.

and

P. Kealy⁴

Airbus Operations UK Ltd, Filton, Bristol BS99 7AR, U.K.

Tow-steered composites are optimized for use in tailoring the aeroelastic behavior of a simple 2D composite wing, with particular emphasis on improving both flutter / divergence airspeeds and gusts loads. Symmetric lay-ups are considered where the fibers vary in orientation along the wing span and chord. Tow-steered laminates were found to increase the instability airspeed by up to 7% compared to optimized straight-fiber laminates, and by 13% compared to optimized laminates with standard ($0^\circ/\pm 45^\circ/90^\circ$) plies. Tow-steered laminates were also found to reduce the peak wing root gust loads (up to 52%) and the correlated gust loads (up to 24%). The lowest gust loads were reached with higher-order nonlinear fiber angle variations when either all plies were optimized or when two-dimensional fiber angle variations were used. Optimization strategies which allowed the fiber angles to vary freely in each ply generally performed better than optimizations based on the rotation of ($0^\circ/\pm 45^\circ/90^\circ$) ply stacks along the span of the wing.

Nomenclature

α	=	local wing section angle of attack
C	=	wing chord
D_{11}, D_{16}, D_{66}	=	Classical Laminar Theory D-matrix stiffness terms
E_1, E_2	=	composite lamina longitudinal and transverse Young's moduli

¹ Ph.D. Research Student – Industrial Case Award, AIAA Student Member

² Royal Academy of Engineering Airbus Sir George White Professor of Aerospace Engineering, AFAIAA

³ Professor in Lightweight Structures

⁴ Loads and Aeroelastics Engineer

EI	= beam bending stiffness parameter
F	= correlated wing root gust load function
g	= damping ratio
G_{12}	= composite lamina in-plane shear modulus
GJ	= beam torsional stiffness parameter
K	= beam bending-torsion stiffness coupling parameter
L	= Legendre polynomials
$M_{\dot{\theta}}$	= unsteady pitch velocity term of the aerodynamic wing section moment
ν_{12}	= composite lamina Poisson's Ratio
ω	= vibration mode frequency
P_{α}	= optimization penalty parameter associated with a wing section angle of attack constraint
$P_{V_{max}}$	= optimization penalty parameter associated with an instability airspeed constraint
q	= Rayleigh-Ritz generalized coordinates
Q, M, T	= wing root gust loads (shear force, bending moment and torque respectively)
ρ_0	= composite lamina average density
R	= optimization objective function scaling parameters
S	= wing span
t	= time
τ	= composite lamina thickness
θ	= local fiber angle relative to the x-direction
T_{mn}	= fiber angles defined at $(M * N)$ equally spaced reference points
V	= airspeed
V_{design}	= design airspeed
V_{max}	= lowest flutter or divergence instability airspeed
w	= local wing deflection in z-direction
x, y, z	= orthogonal coordinate system fixed to wing root
ξ, η	= normalized coordinates along the span (x-direction) and chord (y-direction)

I. Introduction

The aim of aeroelastic tailoring is to improve the aircraft performance in a passive manner, by concurrently optimizing the structural and aerodynamic behaviors. Significant work has been done in the area of aeroelastic tailoring of composite wing structures since the early 1980s. It was first demonstrated on the X-29 experimental aircraft, where a washout effect (wing up-bend coupled to nose-down twist) was used to increase the divergence speed of the forward-swept wing [1,2]. Other aeroelastic tailoring objectives include: weight reduction [3], drag reduction [4], improved gust response [5,6], optimum flutter characteristics [7], and combinations thereof [8-10]. All of these typically involve modifying the stiffness of the wing and the passive elastic coupling between wing bending and torsion deformations, such as to improve the static and dynamic wing behavior in different airflows. With composite wing structures, the fiber angles and layup sequences can be tailored to optimize the stiffness and bending-torsion coupling over the span of the wing.

New aircraft designs are constantly being explored, including high aspect ratio flexible wings, blended wing-body aircraft, morphing wings and also natural laminar flow low-sweep wings [11,12]. To become feasible, these concepts rely on a multidisciplinary design optimization (MDO) approach, of which the aeroelastic tailoring of advanced composite structures could be a key enabler [13,14]. However, the potential benefits of aeroelastic tailoring may currently be diminished due to the limited design space available with standard unidirectional (UD) laminates, which tend to be homogenized orthotropic $0^\circ/\pm 45^\circ/90^\circ$ ply laminates. In order to change the stiffness or bending-torsion coupling of such a UD laminate, either the whole ply stack has to be rotated relative to the part, or plies of specific fiber orientations have to be added or dropped. The second approach introduces offsets and fiber discontinuities, which lead to detrimental stress concentrations and tend to reduce the strength of a laminate [15]. Design rules are typically used to ensure such features are spread-out and are unlikely to cause significant stresses [16]. Traditionally, the use of these standard laminates has been driven by the aircraft certification requirements, where laminates with plies at 3 or more angles are seen to be beneficial in cases of load uncertainty and where the use of a few discrete ply angles for all components means that the amount of material testing to support certification is reduced [17]. However, these constraints could be relaxed in the future if trends towards more accurate and robust analysis methods and more virtual testing continue [18,19].

Over the last twenty years, so called “tow-steering” techniques have been developed to manufacture laminates with variable angle tow (VAT) plies (also called variable-stiffness plies), including automatic fiber placement (AFP),

tailored fiber placement (TFP) and continuous tow sheering (CTS) [20]. The fibers in these plies are locally unidirectional through the thickness of the ply (as opposed to multi-axial, woven or braided materials), but they follow predefined curvilinear paths within the plane of each ply, such that the fiber angles and ply stiffness vary continuously. To simplify the terminology, we will refer to laminates with constant fiber angles in each ply (i.e. straight fibers) as UD laminates, and laminates with variable fiber angles in some or all plies as VAT laminates.

It has been demonstrated that the curvilinear fiber paths can be optimized to increase the structural performance of VAT laminates beyond that of equivalent UD laminates. Analytical and experimental studies have shown that the buckling strength and post buckling-behavior of VAT flat panels can be improved by redistributing the loads in a panel [21-25]. Other studies have demonstrated that stress concentrations around geometrical discontinuities such as cut-outs can be reduced by steering fibers around the discontinuity [26,27], and the change in vibration frequency as a function of the ply angle variation has also been studied [28-31]. The use of VAT composites has even been investigated for wing morphing applications [32]. However, there has been very little work published on the use of VAT composites for aeroelastic tailoring. Recent work by Haddadpour [33] describes a tool used to optimize the flutter speed of a thin-walled idealized beam wing structure with UD and VAT laminates. The analysis results seem to indicate that higher flutter speeds are achievable by using VAT laminates. Also, recent work by the authors [34] investigated the use of tow-steered composites for influencing the aeroelastic behavior of an idealized wing using a simple composite plate model coupled with modified strip theory aerodynamics. It was shown that it is possible to influence the divergence speed, flutter speed and gust response by changing the fiber angle variations along the span.

More generally, the design space for VAT laminates can be further increased by defining 2D fiber angle variations for each VAT ply and also by defining higher order nonlinear fiber angle variations. One approach for modelling more complex VAT laminates is to use a Finite Element based method, in which the variables are defined at each node [31]. However, in this case, additional constraints are often required to ensure that the variations of design parameters between nodes are smooth. Alternatively, VAT laminates can be described using mathematical functions (e.g. B-splines, Lobatto polynomials, Lagrange polynomials) defining either the tow paths or the variations in the fiber angle direction [35]. Different optimization methods have been investigated for VAT laminates. A review of optimization methods for VAT and UD laminates is available in References [36] and [37], with Genetic Algorithms (GA) being one of the most popular methods. Although GAs can be computationally expensive, they can be used for problems with nonlinearities, discontinuous variables or objective functions, as gradient information is not required. GAs can

also be combined with model reduction methods or response surface methodologies to optimize VAT laminates with fewer numbers of sampled points [38].

In this paper, the preliminary work of [34] is extended and enhanced to consider higher order fiber angle variations in one and two-dimensions. The results of single objective optimization studies are assessed, first determining laminates that maximize flutter or divergence instability airspeeds and then laminates that minimize peak gust loads. Then the outcomes from a multi-objective optimization study are evaluated, aiming to determine the optimum laminate for simultaneously minimizing the correlated gust loads at two different design airspeeds, with constraints on the lowest instability airspeed and the maximum plate twist angle. The benefit of using tow steering is evaluated by comparing the aeroelastic performance of the optimized tow-steered laminates to the performance of the optimized standard UD laminates.

II. Wing Model Description

A. Structural Model

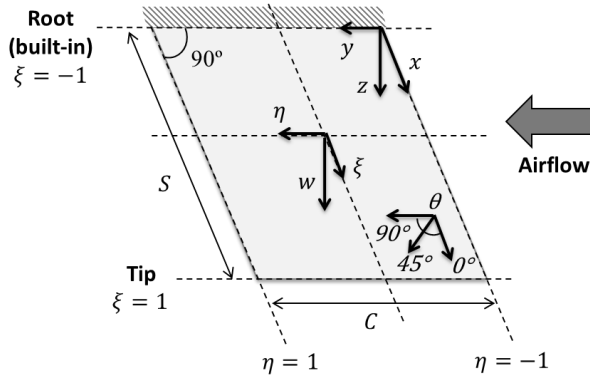


Table 1. Plate geometry and material parameters

Property	Value
E_1	98000 MPa
E_2	7900 MPa
G_{12}	5600 MPa
ν_{12}	0.28
Span, S	304.8 mm
Chord, C	76.2 mm
Density, ρ_0	1520 kg/m ³
Ply thickness, τ	0.134 mm

Figure 1. Simple rectangular wing model of span S and chord C

The structural model used was a modified version of that previously described in [34]. A Rayleigh–Ritz type approach with 8 bending and 8 torsion shape functions was used to approximate the structural behavior of the simple rectangular plate wing shown in Figure 1. The wing dimensions and material properties are listed in Table 1. The wing was assumed to be chordwise rigid and therefore behaved like a beam, which is representative of the behavior of wing skins supported by closely spaced ribs [39]. Only symmetric laminates were considered, which simplified the analysis by avoiding bending-extension coupling effects. The plate was assumed to consist of a perfectly bonded stack of plies,

with infinitely thin and stiff bondlines. The displacements were therefore continuous across the ply boundaries; small deflections and linear material behavior were also assumed.

The tow-steered fiber angle variation definition was updated to allow for higher order fiber angle variations over the span of the plate (1D) and both over the span and chord of the plate (2D). The updated fiber angle variation $\theta(\xi, \eta)$ was based on Lagrange polynomials [25], such that

$$\theta(\xi, \eta) = \sum_{m=0}^{M-1} \sum_{n=0}^{N-1} T_{mn} \cdot \prod_{m \neq i} \left(\frac{\xi - \xi_i}{\xi_m - \xi_i} \right) \cdot \prod_{n \neq j} \left(\frac{\eta - \eta_j}{\eta_n - \eta_j} \right) \quad (1)$$

where T_{mn} are the fiber angles defined at $(M * N)$ equally spaced reference points on the plate with coordinates (ξ_m, η_n) and (ξ_i, η_j) and where ξ and η are the normalized coordinates along the span and chord of the wing defined over $[-1, 1]$ as shown in Figure 1. For a 1D linear fiber angle variation along the span of the wing, Eq.(1) reduces to

$$\theta(\xi) = (T_1 - T_0) \left(\frac{\xi + 1}{2} \right) + T_0 \quad . \quad (2)$$

Lagrange polynomials were used to guaranty that the input fiber angles at each reference point were actually enforced on the plies, although there was no direct control on the fiber angle variations between reference points. Lagrange polynomials also ensured that each additional reference point along the span or the chord of the wing increased the order of the fiber angle variation by 1. Other interpolation methods such as B-splines or Bezier-splines, which allow generally less control, may have been preferred if more than 5 reference points had been used, since Lagrange polynomials can result in undesired rapid fluctuations for large numbers of reference points. The results in section III show that the behaviors of optimized VAT solutions can be similar despite differences in the fiber angle variations, which indicates that the particular fiber angle interpolation method chosen may become less significant as the design space is increased.

To avoid ill-conditioning, a quasi-Monte Carlo numerical integration method [40] was implemented along with shape functions based on Legendre polynomials, which have good convergence characteristics [41], such that

$$w(\xi, \eta) = \sum_{m=1}^8 \sum_{n=1}^2 q_{mn} (1 + \xi)^2 L_m(\xi) L_n(\eta) \quad (3)$$

where the Legendre polynomials are defined as

$$L_0(\xi) = 1; \quad L_1(\xi) = \xi; \quad L_2(\xi) = \frac{1}{2}(3\xi^2 - 1); \quad \dots$$

$$L_i(\xi) = \sum_{j=0}^i (-1)^j \frac{(2i-2j)!}{2^j j! (i-j)! (i-2j)!} \xi^{i-2j} \quad (4)$$

with $J = \frac{i}{2}$ ($i = 0, 2, 4, \dots$), $\frac{i-1}{2}$ ($i = 1, 3, 5, \dots$)

It was verified that the model with 16 shape functions accurately captured the normal modes of a number of different test layups by performing a convergence study on the number of assumed shape functions and by comparing the results with Finite Element Model predictions (Table 2).

Table 2. Convergence study on the first five free vibration frequencies (Hz) as a function of the number of assumed shape functions for two test layups

Layup	Mode	Number of assumed shape functions (DoF)				FEM
		8	12	16*	20	
[45 45 0]s	1st bending	5.0	4.9	4.9	4.9	4.9
	2nd bending	31.5	30.4	30.4	30.4	30.4
	1st torsion	74.9	73.8	73.8	73.8	72.8
	3rd bending	95.3	85.5	85.5	85.5	85.7
	4th bending	232.1	185.8	170.4	170.0	170.8
[0 0 90]s	1st bending	11.1	11.1	11.1	11.1	11.1
	1st torsion	39.7	39.6	39.6	39.6	40.1
	2nd bending	69.8	69.4	69.4	69.4	69.4
	2nd torsion	133.7	133.4	133.4	133.4	134.5
	3rd bending	199.6	194.5	194.4	194.4	195.0

*selected number of shape functions

For the optimization studies, the EI/GJ/K beam stiffness parameters [39] were extracted to compare the various optimum laminates. These values were calculated from the standard laminate stiffness matrix terms as

$$EI = CD_{11} \quad ; \quad GJ = 4CD_{66} \quad ; \quad K = 2CD_{16} \quad . \quad (5)$$

B. Aeroelastic Model

The aeroelastic modelling approach was the same as that used in Reference [34]. The quasi-steady aerodynamic forces on the wing were calculated using modified strip theory and an additional unsteady pitch velocity term ($M_{\dot{\theta}} = 1.2$) was included in the quasi-steady pitching moment equation to improve flutter and gust behavior predictions, where $M_{\dot{\theta}}$ is effectively an approximation to the Theodorsen function moment derivative based on an average value over a range of reduced frequencies and flexural axis positions [42]. Despite its limitations, the model was found to capture the aeroelastic behavior of a simple high aspect-ratio wing at low subsonic airspeeds with sufficient accuracy

to allow a comparison between the UD/VAT optimized laminates; this was previously verified by comparing the model predictions with Finite Element Model results in Reference [34]. It should be emphasized, that the aim here is not to predict the wing response with high accuracy, but to compare representative behaviors obtained using the same model, where modelling inaccuracies would affect both UD and VAT laminate wing behaviors in equal measure.

The flutter and the divergence airspeeds were determined, as well as the vibration frequencies, mode shapes and damping as a function of airspeed. The effect of a discrete (1-cosine) gust on the cantilevered plate was also analyzed in the time domain by including the lift force and pitching moments due to the gust in the aeroelastic system equation.

To simplify the equations, the root angle of attack of the plate was set to zero, which means that there were no steady state aerodynamic loads acting on the plate. Aerodynamic loads were therefore uniquely generated by small disturbances in the airflow for the flutter and divergence analyses and by the oncoming vertical air velocity for the gust analysis.

III. Wing Laminate Optimization

Optimization studies on an 8-ply symmetric laminate were performed to determine optimum fiber angle distributions for different aeroelastic tailoring objectives. In a first study, the fiber angle distributions for maximum instability airspeed (flutter or divergence) were determined. In a second study, the fiber angle distributions for minimum gust load peaks were determined. Finally, a multi-objective optimization study was performed, aiming to determine the optimum laminate for simultaneously minimizing the time-correlated gust loads at two different design airspeeds, with constraints on the lowest instability airspeed and the maximum plate twist angle. In each case the optimum solutions were identified and their aeroelastic characteristics explored. Finally the value and limitations of these studies are reviewed.

The optimization variables consisted of the string of integer valued fiber angles at each reference point and for every ply. For example, the optimization of an 8-ply symmetric laminate with a spanwise fiber angle variation of order 4 (5 reference points) resulted in an input string of 20 fiber angles. The fiber angles at reference points were defined at 5° increments between -90° and $+90^\circ$.

For all optimization studies, the integer GA available in Matlab with random initial sub-populations was used [43] (typically 6 sub-populations with 50 individuals each, evolved over at least 200 generations). Although GAs are very good at finding global optimal solutions in highly multi-modal design spaces, they do not allow the convergence to a

global solution to be analytically verified. Therefore, each optimization was repeated at least 5 times and it was verified that the runs found optimal solutions with similar fitness values, although it was frequently found that several different optimal fiber angle variation solutions (weakly dominated to each other) may exist.

Three different laminate optimization parameters were explored. The first parameter was the number of plies that were being optimized in the laminate, either only the 4 outer plies or all 8 plies. This parameter reflects the choice between an ideal full laminate optimization and a practical laminate optimization approach, where only the outer plies are tailored since they have the largest effect on the plate's bending and bend-twist coupling stiffness (second moment of area effect). Using the practical optimization approach, not only are the number of design variables halved, but the inner ply stack could also be designed such as to fulfill other functions (e.g. strength requirements). The second parameter was the order of the fiber angle variation in the optimized plies, from an order of 0 (UD laminate optimization) to an order of 4 (quartic fiber angle variation). The third parameter was the dimensionality of the fiber angle variation, where a 1D variation corresponds to fiber angles only changing along the span of the wing and a 2D variation corresponds to fiber angles changing both along the span and chord of the plate. For 2D variations, for simplicity, the order of the fiber angle variation was set to be the same along the span and the chord of the wing. The effect of changing these parameters was evaluated by comparing the results of four different design optimization strategies:

- (1) optimization of the 4 outer plies only, with 1D fiber angle variations of order 0 to 4;
- (2) optimization of all 8 plies, with 1D fiber angle variations of order 0 to 4;
- (3) optimization of the 4 outer plies only, with 2D fiber angle variations of order 0 to 4;
- (4) optimization of all 8 plies, by rotating an optimized stack of $(0^\circ/\pm 45^\circ/90^\circ)$ plies in 1D, with fiber angle variations of order 0 to 4. There was no constraint to keep the laminate locally balanced and it was generally found that the optimizer would select laminates which did not have the same number of $+45^\circ$ and -45° plies.

For optimization strategies (1) and (3) an arbitrary (non-optimized) inner ply stack of $[-45^\circ +45^\circ]_s$ was used.

A. Flutter and Divergence Airspeed Optimization

Table 3. Maximum optimized instability airspeeds (m/s) as a function of the order of the fiber angle variation and of the laminate optimization strategy

Optimization strategy	Order of the fiber angle variation				
	0	1	2	3	4
(1)	68	71	76	76	76
(2)	71	73	76	76	76
(3)	68	72	76	76	75
(4)	67	71	74	73	74

The first optimization study aimed to determine the optimal fiber angle distributions for maximizing the wing's lowest flutter or divergence instability airspeed. The maximum instability airspeeds achieved by each of the four tow-steered design strategies are summarized in Table 3 as a function of the order of the fiber angle variation. The lowest optimum (67m/s) was found with the 8 ply stack rotation of order 0, which corresponds to a standard UD laminate optimization with plies of $0^\circ/\pm 45^\circ/90^\circ$ fiber angles. The highest optimum (76m/s) was achieved with each of the three VAT optimization strategies (1) to (3) with at least quadratic fiber angle variations.

To illustrate how the VAT laminates can be tailored to increase the instability airspeed compared to UD laminates, the structural properties and the V_g and V_ω graphs for optimized UD and VAT laminates from optimization strategy (1) are plotted in Figure 2 and Figure 3. In these figures, the flexural axis is defined as the locus of flexural centers along the span of the wing at which an applied out-of-plane force causes only bending and no rotation of the section on which the force is applied relative to the wing root [44].

For the optimized UD laminate, the torsional stiffness (GJ) was approximately two times larger than the bending stiffness (EI) (Figure 2). This was beneficial, because it reduced the second bending mode frequency (mode 2) below the first torsional mode frequency (mode 3) and prevented low airspeed flutter due to an interaction of the first bending and first torsion modes. Moreover, since the outer-ply fiber angle was negative, the flexural axis was swept forward towards the leading edge of the wing, which increased the divergence airspeed (washout effect). However, the forward location of the flexural axis also reduced the damping of the first bending mode, which then interacted with the second bending mode and lead to flutter at 68m/s. It should be noted that both bending vibration modes included some torsional deflections due to the bending-torsion coupling of the laminate.

In comparison, the VAT laminate in Figure 3 achieved a high torsional stiffness inboard while maintaining a flexural axis close to the half-chord location. This effectively damped-out the first bending mode at 64m/s, preventing

flutter due to interactions with this mode. Outboard, the outer ply fibers swept forward, reducing the local torsional stiffness, which decreased the amount of energy absorbed by the first torsion mode. This occurrence prevented the first torsion mode from becoming unstable and increased the flutter airspeed due to the interaction of modes 2 and 3 to 76m/s, where the second bending mode became unstable. This was followed by mode 1 divergence at 77m/s; characterized by the fully damped mode 1 suddenly becoming unstable. This is a static aeroelastic phenomenon, where the applied aerodynamic forces overcome the restoring elastic forces, leading to an infinite increase in the airfoil angle of attack and therefore wing failure.

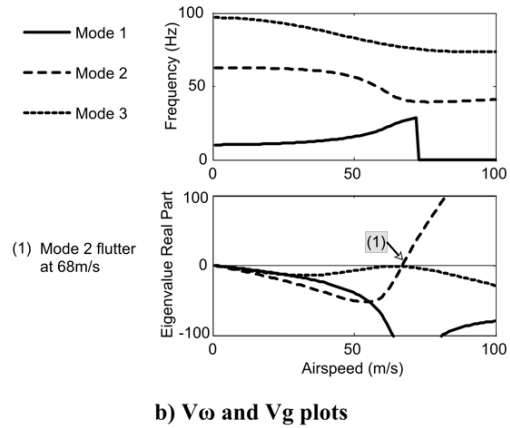
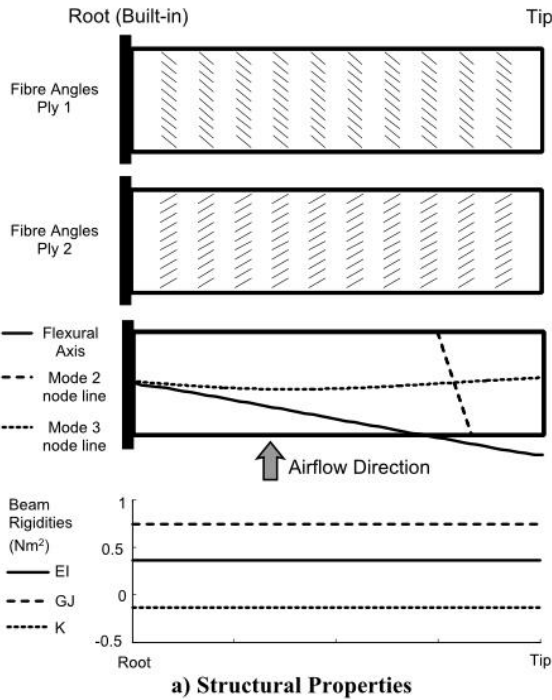


Figure 2. Optimum UD laminate solution from optimization strategy (1) (Ply 1 = outer ply)

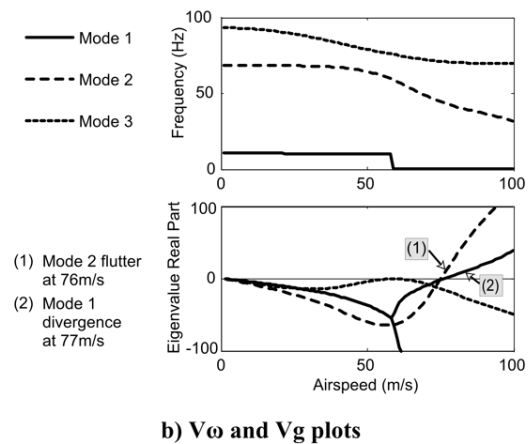
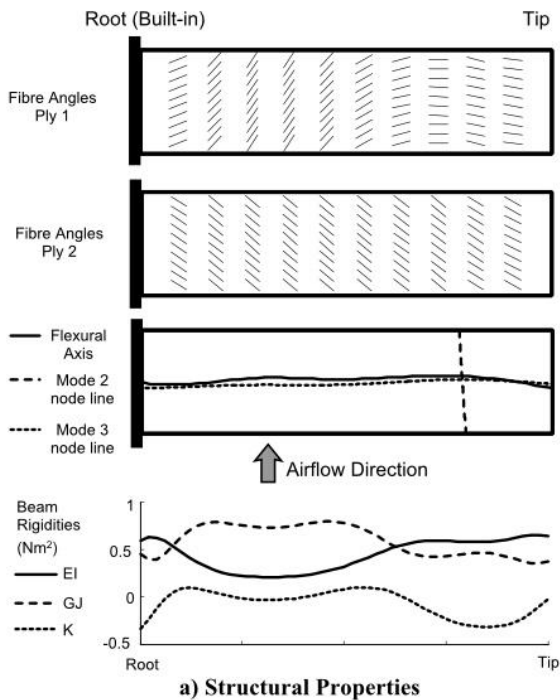


Figure 3. Optimum VAT laminate solution from optimization strategy (1) for a fiber angle variation of order 4 (Ply 1 = outer ply)

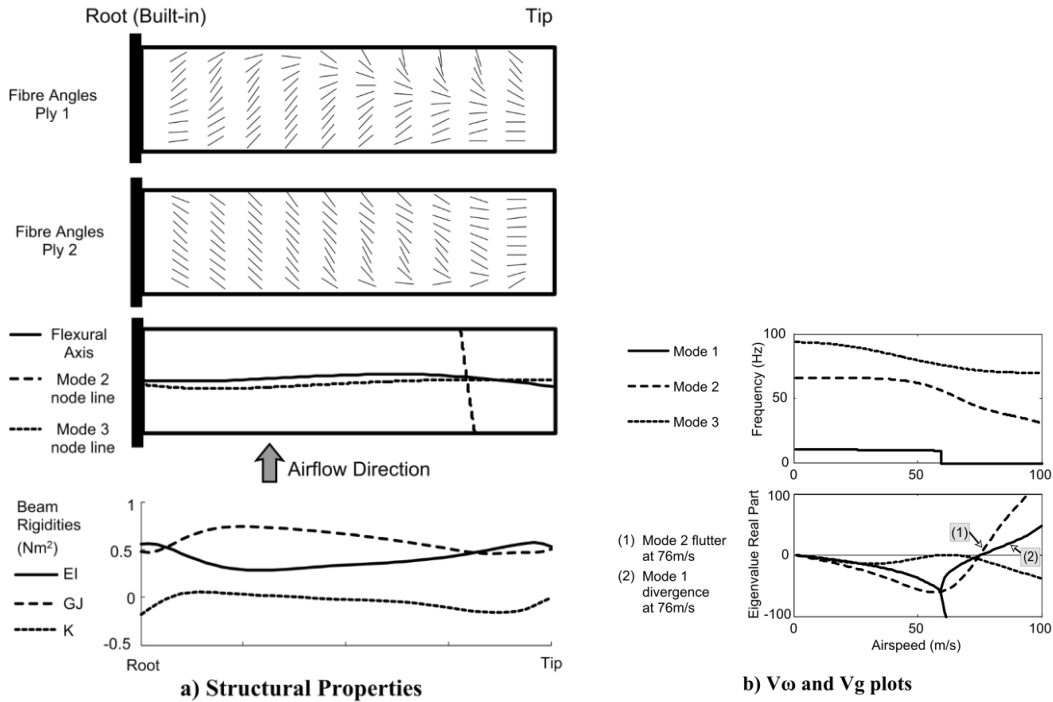


Figure 4. Optimum VAT laminate solution from optimization strategy (3) for a fiber angle variation of order 3 (Ply 1 = outer ply)

For this study, the relatively good performance of design strategy (1) was due to two main factors. The first was that the plate behavior can be improved by only optimizing the fiber angles in the outer plies. This follows from classical laminate theory, where the contribution of each ply to the laminate bending/torsion stiffness increases with the cube of the ply distance from the laminate mid-plane (second moment of area effect). The second factor was that the arbitrarily chosen stack of $[-45^\circ +45^\circ]_s$ inner plies was fortuitously close to one optimum solution for these plies from optimization strategy (2). The results from strategy (3) indicate that no significant advantage may be gained from using 2D vs. 1D fiber angle variations in this case; indeed, the stiffness distributions and the aeroelastic behaviors in Figures 3 and 4 are very similar, despite the different fiber angle distributions. For strategy (3), it should also be noted that the GA algorithm failed to converge for fiber angle variations of order 4 due to the decrease in the convergence rate of the GA. Further work therefore should investigate how to improve the convergence behavior as the number of fiber angle variables increases. Strategy (4) had the worst performance, since it did not allow the variations in bending and torsional stiffness along the span to be decoupled.

B. Gust Load Optimization

The second optimization study determined the optimum fiber angle distributions for minimizing the peak gust loads on the wing. In practice, the gust intensity and lengths are defined by the certification authorities [45]. However, due to the size of the wing model (<1m span) and its relatively high natural frequencies, these standard definitions were not appropriate. For this study, a discrete (1-cosine) gust of 1m length and 1m/s upwards vertical velocity was applied at two different design airspeeds of 20m/s and 60m/s. The effective wing root shear load (Q), bending moment (M) and torque (T) were minimized separately, such that each optimization analysis minimized only one of the following fitness functions at one design airspeed:

$$Fitness = Q + P_{V_{max}} + P_{\alpha} \quad \text{or} \quad Fitness = M + P_{V_{max}} + P_{\alpha} \quad \text{or} \quad Fitness = T + P_{V_{max}} + P_{\alpha}$$

where

$$Q = \sqrt{\max(Q(t))^2 + \min(Q(t))^2} \quad ; \quad M = \sqrt{\max(M(t))^2 + \min(M(t))^2} \quad ;$$

$$T = \sqrt{\max(T(t))^2 + \min(T(t))^2}$$

$$P_{\alpha} = \begin{cases} \frac{V_{max} - (1.1 * V_{design})}{1.1 * V_{design}} * 1000 & \text{if } V_{max} < (1.1 * V_{design}) \\ 0 & \text{otherwise} \end{cases} \quad (6)$$

$$P_{\alpha} = \begin{cases} \frac{\alpha_{max} - 5}{5} * 1000 & \text{if } abs(\alpha(\xi, t)) > 5^{\circ} \\ 0 & \text{otherwise} \end{cases}$$

with

$$\xi \in [-1,1] \quad ; \quad t \in [0,0.3]s \quad ; \quad V_{design} = 20m/s \quad \text{or} \quad 60m/s$$

A first penalty parameter ($P_{V_{max}}$) was introduced to ensure that the lowest flutter or divergence instability airspeed was at least 10% higher than the design speed. A second penalty parameter (P_{α}) ensured that the wing rotation did not exceed 5° at any location along the wing. Both penalty parameters increased rapidly with increased distance from feasible solutions, such that the optimization algorithm would quickly converge towards feasible solutions.

The optimization results for the two different design airspeeds are summarized in Table 4 and Table 5 as a function of the order of the fiber angle variation. These results show that by using VAT laminates, the discrete gust loads can be reduced by up to 52% at 60m/s and up to 22% at 20m/s compared to optimized UD laminates.

Table 4. Minimum optimized wing root gust loads Q, M and T (normalized) as a function of the optimization strategy and the order of the fiber angle variation for a design airspeed of 20m/s

Opt. strategy	Q					M					T				
	Order of the fiber angle variation					Order of the fiber angle variation					Order of the fiber angle variation				
	0	1	2	3	4	0	1	2	3	4	0	1	2	3	4
(1)	(1)*	0.82	0.82	0.82	0.81	(1)*	0.88	0.87	0.85	0.84	(1)*	0.98	0.96	0.96	0.95
(2)	1.00	0.78	0.78	0.78	0.78	0.96	0.81	0.80	0.78	0.78	0.99	0.95	0.92	0.92	0.91
(3)	(1)*	0.82	0.81	0.81	0.80	(1)*	0.86	0.84	0.83	0.83	(1)*	0.97	0.95	0.95	0.94
(4)	1.00	0.79	0.78	0.78	0.78	0.96	0.83	0.81	0.78	0.78	0.99	0.94	0.92	0.92	0.91

*baseline

Table 5. Minimum optimized wing root gust loads Q, M and T (normalized) as a function of the optimization strategy and the order of the fiber angle variation for a design airspeed of 60m/s

Opt. strategy	Q					M					T				
	Order of the fiber angle variation					Order of the fiber angle variation					Order of the fiber angle variation				
	0	1	2	3	4	0	1	2	3	4	0	1	2	3	4
(1)	(1)*	0.67	0.65	0.64	0.63	(1)*	0.67	0.66	0.53	0.52	(1)*	0.80	0.78	0.79	0.75
(2)	0.96	0.65	0.61	0.55	0.52	0.95	0.58	0.54	0.50	0.48	0.95	0.79	0.77	0.74	0.73
(3)	(1)*	0.64	0.68	0.63	0.61	(1)*	0.65	0.57	0.53	0.53	(1)*	0.77	0.75	0.74	0.77
(4)	0.96	0.81	0.77	0.75	0.76	0.95	0.84	0.78	0.78	0.77	0.95	0.83	0.77	0.77	0.78

*baseline

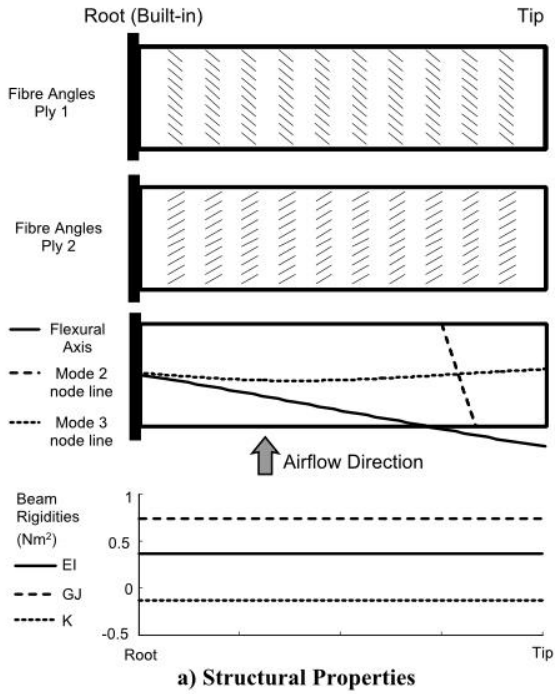
To illustrate how the VAT laminates were tailored to reduce the gust loads compared to the UD laminates, the structural properties and the gust response of optimized UD and VAT laminates from strategies (1) and (3) are plotted in Figures 5-7. All laminates minimized the root bending moment (M) at 60m/s. The root bending moment was calculated by integrating the shear load distribution over the span of the wing, which included the aerodynamic forces (gust forces and forces induced by the heave and pitch response of the plate) and inertia forces. The usual convention of positive shear forces in the negative z-direction (as per Figure 1) was adopted (i.e. lift is positive up). The lowest instability airspeed was 68m/s for the UD laminate and 66m/s for both VAT laminates, and the plate twists did not exceed 5°; therefore, all three designs were feasible and penalty parameter values were zero.

Both optimized VAT laminate wings have similar gust responses, despite differences in the fiber angles and stiffness distributions. This shows that multiple optimal solutions (weakly dominated to each other) may be found using VAT laminates.

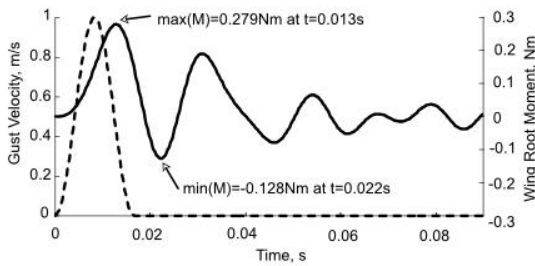
The maximum root bending moment ($max(M)$) was due to the cumulative effect of the gust forces and the wing response. The VAT laminates reduced this moment by delaying the peak vibration response relative to the peak applied gust velocity. This was achieved by a reduction in the bending and torsional stiffness (EI and GJ) of the VAT laminates compared to the UD laminate, particularly at the root and tip of the wing.

The minimum root bending moment ($min(M)$) was only driven by the wing response (since the gust velocities were zero at that time step). The gust mainly excited the second bending mode of the laminates, which resulted in negative inertia shear forces in the inboard section and positive inertia in the outboard section at the minimum root bending moment time step. The positive inertia forces bent the wing tip up and twisted the leading-edge down due to the offset between the flexural axis and the mass axis (at half-chord). For the VAT laminates, this effect was beneficial at the wing tip, where the twist-induced negative aerodynamic forces compensated for the positive inertia forces. However, for the UD laminate, the flexural axis was too far forward, which caused not only the outboard but also the inboard leading edge to twist down and induced detrimental negative aerodynamic loads in the inboard section. Although the VAT laminates' twist deflections are relatively small compared to that of the UD laminate, it should be highlighted that the VAT laminates' lower bending stiffness resulted in overall larger tip deflection magnitudes compared to the UD laminate (25mm, 23mm and 17mm respectively at the $min(M)$ time step).

For this study, optimization strategies (2) and (3) generally reduced the gust loads more than strategy (1), by either tailoring the inner ply stack (strategy (2)) or by more accurately tailoring the EI/GJ/K stiffness contributions of each ply (strategy (3)). The good performance of strategy (4) at 20m/s is due to the fact that the optimum solutions from all strategies at 20m/s have similar fiber angle variations in the two outer plies. However, strategy (4) is no longer competitive at 60m/s, where the optimum solutions require the independent variation of the fiber angles in the two outer plies (as illustrated in Figure 6).

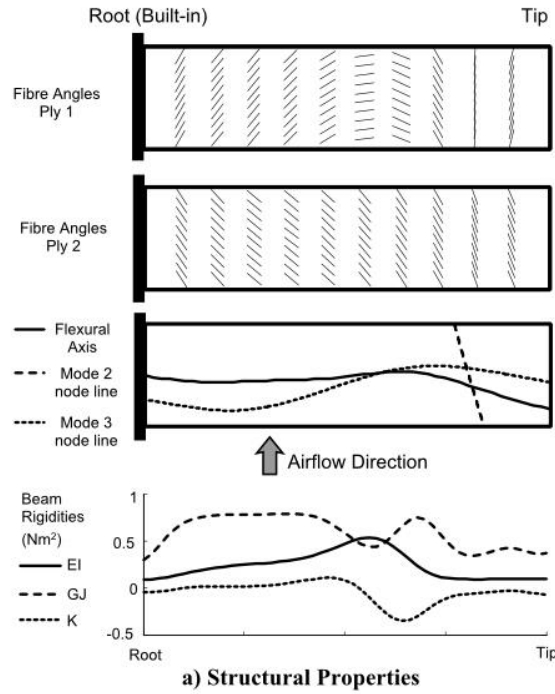


a) Structural Properties

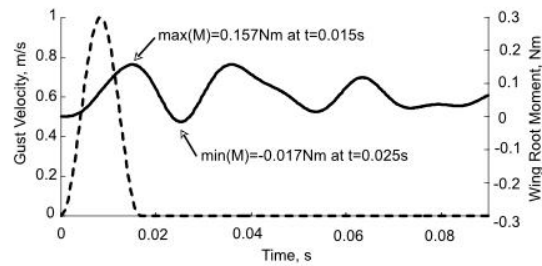


b) Gust Response and Shear Load Distribution

Figure 5. Optimum UD solution from strategy (1) for minimizing the root bending moment at 60m/s (Ply 1 = outer ply)



a) Structural Properties



b) Gust Response and Shear Load Distribution

Figure 6. Optimum VAT solution from strategy (1) for minimizing the root bending moment at 60m/s with a fiber angle variation of order 4 (Ply 1 = outer ply)

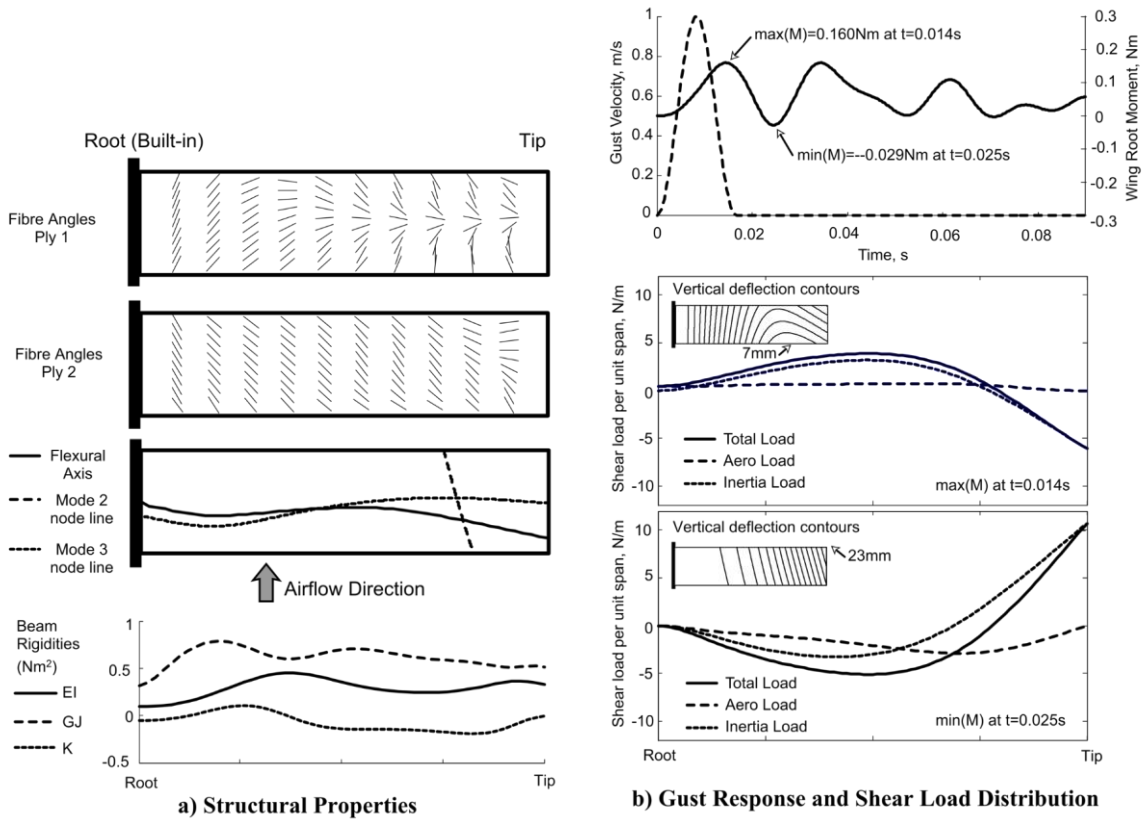


Figure 7. Optimum VAT solution from strategy (2) for minimizing the root bending moment at 60m/s with a fiber angle variation of order 3 (Ply 1 = outer ply) (Critical flutter airspeed = 66m/s)

C. Multi-Objective Aeroelastic Optimization

This study determined the optimum fiber angle distributions for minimizing the correlated gust loads on the wing. For this study, loads were minimized at the same time at 20m/s and 60m/s for a discrete (1-cosine) gust of 1m length and 1m/s upwards vertical velocity. A similar study would have been the optimization of the laminates for different lengths of gusts at a constant design airspeed. As mentioned previously, an arbitrary small gust length and amplitude were used rather than the certification gusts due to the small size of the wing model. The same constraints on instability airspeed (V_{max}) and twist angle (α) were used as in section B.

The multi-objective optimization was performed using a simple normalized objective function weighting scheme. This approach was chosen as it is intuitive and easy to use. Moreover, for problems with convex pareto-fronts, it also guarantees finding solutions on the entire pareto-optimal set [46], defined as the set of solutions which are non-dominated in the entire feasible search space. As shown below, the resulting pareto points were sufficiently closely

spaced to assume such convex pareto-fronts. It should be emphasized that the aim was not to determine the exact pareto front for each laminate optimization strategy, but rather to qualitatively compare the different pareto-fronts obtained using the same optimization algorithm.

The optimization algorithm is minimizing the following fitness function:

$$\begin{aligned}
 & \text{Fitness} = R_1 \cdot \max(F_1) + R_2 \cdot \max(F_2) + P_{V_{max}} + P_\alpha \\
 \text{where} & \\
 F_1 &= \sqrt{(R_{Q1}Q(t))^2 + (R_{M1}M(t))^2 + (R_{T1}T(t))^2} \quad \text{at } V = 20\text{m/s} \\
 F_2 &= \sqrt{(R_{Q2}Q(t))^2 + (R_{M2}M(t))^2 + (R_{T2}T(t))^2} \quad \text{at } V = 60\text{m/s} \\
 & P_{V_{max}} > 0 \quad \text{if } V_{max} < 66\text{m/s} \quad ; \\
 & P_\alpha > 0 \quad \text{if } \text{abs}(\alpha(\xi, t)) > 5^\circ \\
 \text{with} & \\
 & \xi \in [-1,1], t \in [0,0.3]\text{s} \\
 & R_1 + R_2 = 1 \quad \text{with } R_1, R_2 \in [0,1]
 \end{aligned} \tag{7}$$

and $R_{Q1}, R_{Q2}, R_{M1}, R_{M2}, R_{T1}, R_{T2}$ are arbitrary positive scaling parameters, which allow the relative importance of the root shear load, bending moment and torque to be defined. For this study, these parameters are set such that equal importance is attributed to reductions in Q, M and T for both design airspeeds, based on reference values of Q, M and T from optimum UD laminate solutions from section B. The functions $\max(F_1)$ and $\max(F_2)$ correspond to the maximum correlated wing root gust loads at the two airspeeds. By varying the objective function scaling parameters R_1 and R_2 , the trade-off between a reduction in gust loads at 20m/s and one at 60m/s can be established in the form of a pareto-optimal set.

Table 6. Minimum optimized fitness (normalized) as a function of the optimization strategy and the order of the fiber angle variation (for $R_1=R_2=0.5$)

Optimization strategy	Order of the fiber angle variation				
	0	1	2	3	4
(1)	(1)*	0.79	0.79	0.78	0.78
(2)	0.96	0.77	0.77	0.77	0.76
(3)	(1)*	0.78	0.77	0.76	0.78
(4)	0.96	0.90	0.89	0.89	0.88

*baseline

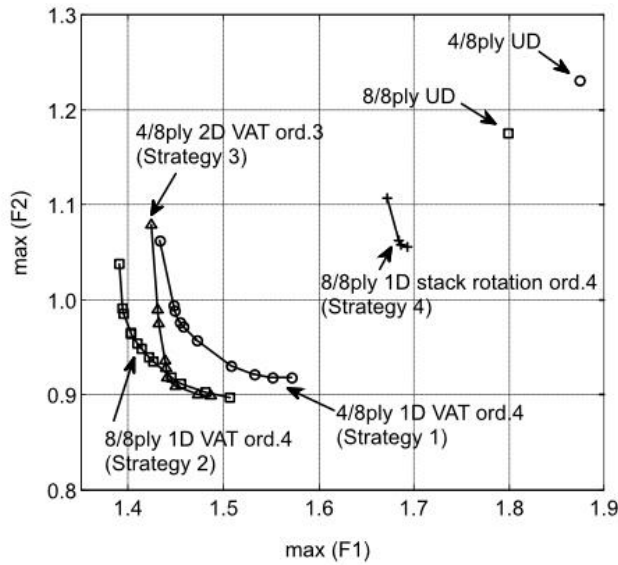


Figure 8. Overview of best pareto fronts for different optimization strategies

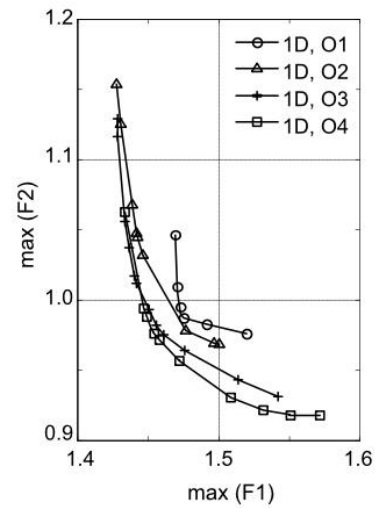


Figure 9. Strategy (1) pareto fronts for fiber angle variations of order 1 to 4

The optimization results are summarized in Table 6, with the optimized VAT laminates leading to a correlated gust load reduction of up to 24% compared to the optimized UD solutions. The pareto-optimal sets for different optimization strategies and for increasing orders of fiber angle variations are plotted in Figure 8 and Figure 9. This shows that the VAT laminates not only allow an overall reduction in loads, but also an increase in the choice of optimal solutions, by allowing a trade-off between gust load reductions at the two design airspeeds.

The structural properties and the gust responses of optimized UD and VAT solutions from strategies (1) and (3) are plotted in Figures 10-12. The lowest instability airspeed was 66m/s for all three laminates and the plate twists did not exceed 5°; therefore, the three designs were feasible and penalty parameter values were zero. Both optimized VAT laminates have again very similar gust responses, despite differences in the fibre angle variations and stiffness distributions. The $\max(F_1)$ and $\max(F_2)$ peaks were mainly due to combinations of high root shear and bending moment loads. As for the previous study (section B), the VAT laminates achieved a reduction in these load peaks compared to the UD laminate by delaying the peak vibration response relative to the peak applied gust velocity. Again, the VAT laminates' bending and torsional stiffness (EI and GJ) were lower than those of the UD laminate, particularly at the root and tip of the wing.

As mentioned in the previous study, a flexural axis location forward of the wing tip leading edge was detrimental in terms of reducing the loads induced by the 60m/s gust. However, at 20m/s, the gust excited mainly the first bending

mode of the wing, where inertia forces were positive at maximum up-bend and negative at maximum down-bend. In this case, a forward location of the flexural axis over the whole wing was beneficial, since it coupled positive inertia forces with negative aerodynamic forces (due to leading-edge down-twist) and the other way around. The optimized VAT laminates were therefore inherently a compromise between reducing the gust loads at one design airspeed at the detriment of increasing the gust loads at the other design airspeed.

This study highlighted the relative performances of the four optimization strategies for the specific case of the simple rectangular plate wing with 8 plies. Strategy (4) had the worst performance, because it only achieved a 12% total load reduction and its pareto-optimal set was small. Strategies (2) and (3) had the best performance relative to their respective 4/8ply and 8/8ply optimum UD solutions, with overall load reductions of 21% and 24% and larger pareto-optimal sets. Arguably, strategy (1) delivered the best compromise between significantly reducing the gust loads (reduction of 22% compared to the 4/8ply UD solution), providing a wide set of pareto-optimal solutions and minimizing the number of design variables, which allowed for a faster, more efficient optimization.

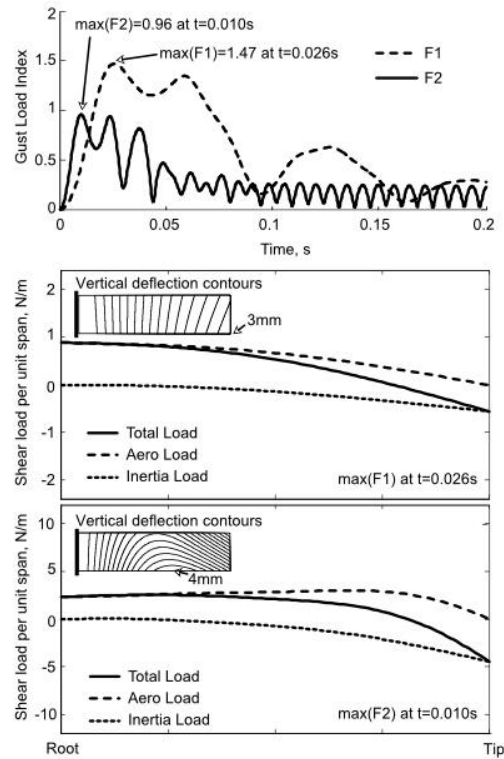
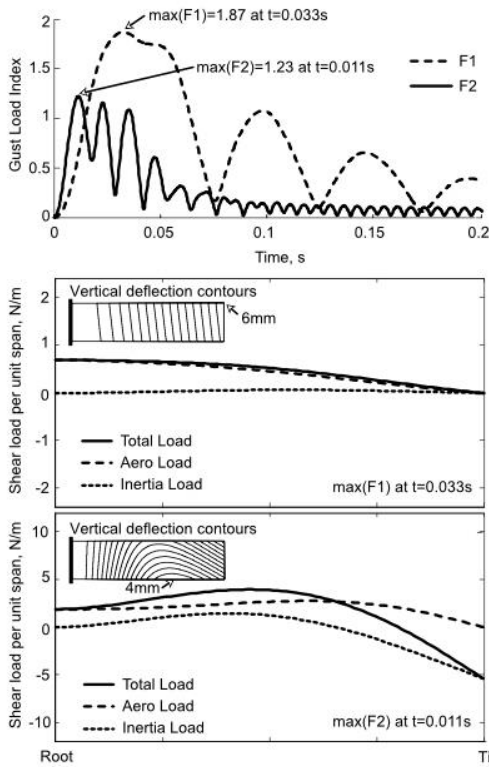
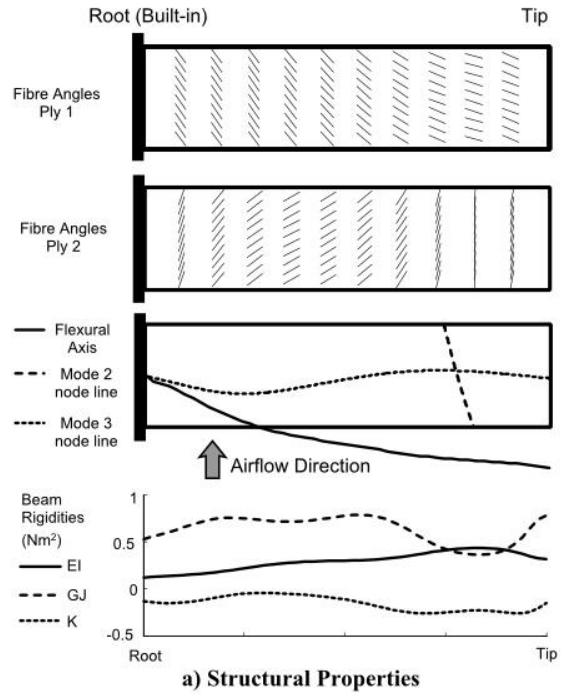
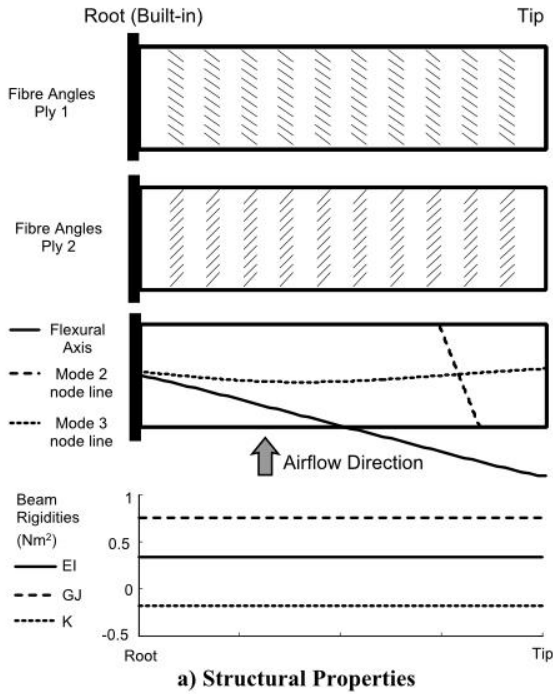


Figure 10. Optimum UD laminate solution from strategy (1) for reducing the correlated gust loads (for $R_1=R_2=0.5$) (Ply 1 = outer ply)

Figure 11. Optimum VAT laminate solution from strategy (1) for reducing the correlated gust loads (for $R_1=R_2=0.5$) with a fiber angle variation of order 4 (Ply 1 = outer ply)

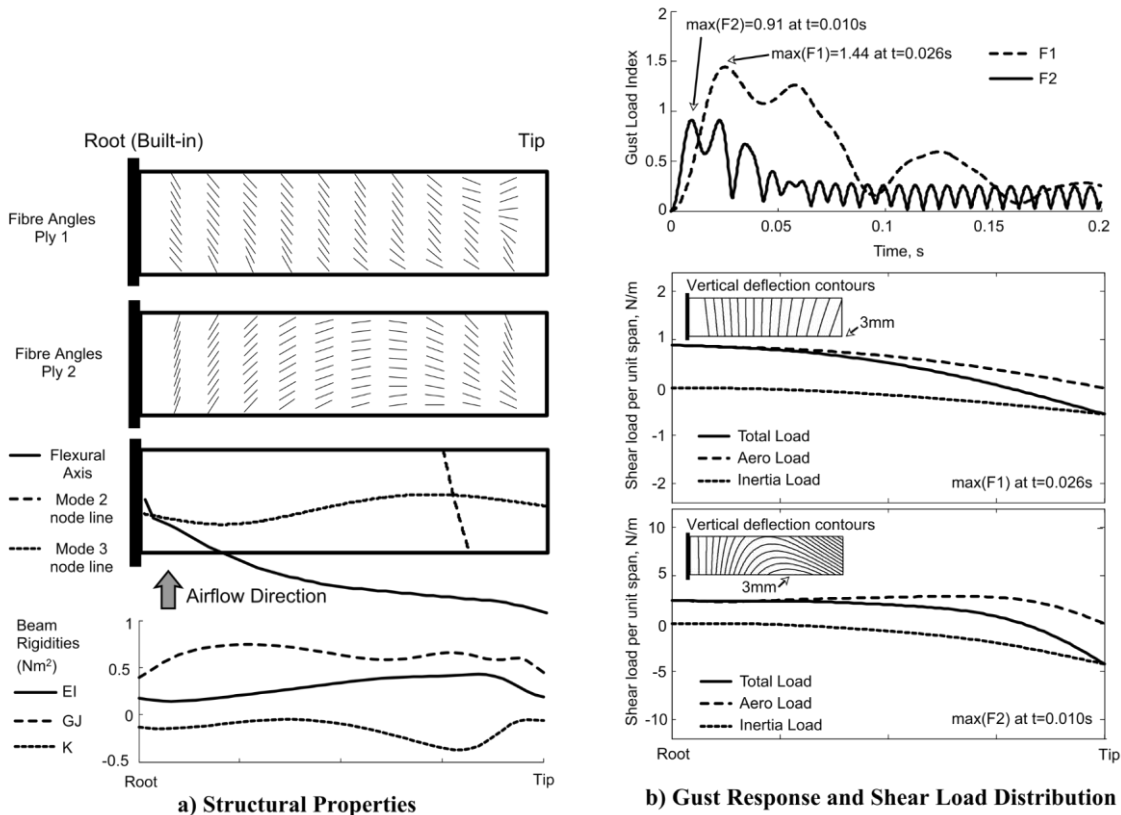


Figure 12. Optimum VAT laminate solution from strategy (3) for reducing the correlated gust loads (for $R_1=R_2=0.5$) with a fiber angle variation of order 3 (Ply 1 = outer ply)

D. Scientific significance and limitations

The optimization studies have shown how 1D and 2D VAT laminates could improve the aeroelastic behavior of a simple wing by continuously changing its stiffness along the span and the chord. It was demonstrated that even 1D, 1st order fiber angle variations could lead to significant gust-load reductions, and that by opening the design space, VAT laminates allowed larger numbers of pareto-optimal solutions. A better understanding of the mechanisms for aeroelastic tailoring with VAT laminates was developed.

Since the results were compiled for the specific case of the simple rectangular plate wing with 8 plies and a limited number of load cases, they cannot be expected to generalize to more complex or different geometry wings. Instead, the rectangular plate optimization can be seen to constitute a first practical step towards a more realistic wing box model optimization, with more realistic load cases and additional structural, mass and control effectiveness

constraints, which will be required in order to determine the benefits of using VAT laminates for aeroelastic tailoring with more accuracy.

IV. Conclusions

The aeroelastic behavior of a simple composite wing was optimized using 8-ply symmetric tow-steered (VAT) laminates in order to investigate the potential for VAT laminates to increase the flutter / divergence instability airspeeds and to reduce the internal loads associated with gusts. An assumed modes model of a simple rectangular unswept composite wing combined with modified unsteady strip theory aerodynamics was used. The fiber angles in each tow-steered ply were defined using Lagrange polynomials, with linear to 4th order fiber angle variations in 1D and 2D. Different optimization strategies were explored, comparing the effect of: 1) varying the number of plies optimized; 2) increasing the order of the fiber angle variation; 3) using 1D or 2D fiber angle variations; 4) rotating a standard ($0^\circ/\pm 45^\circ/90^\circ$) ply laminate in 1D.

Optimum laminates for maximum flutter / divergence speeds and for minimum gust loads were determined and their aeroelastic behavior was reviewed. The VAT laminates increased the instability airspeed by up to 7% compared to optimized UD laminates, and by 13% compared to optimized UD laminates with standard ($0^\circ/\pm 45^\circ/90^\circ$) plies. Compared to optimized UD laminates, VAT laminates also reduced the peak wing root gust loads (up to 52%) and the correlated gust loads (up to 24%). The lowest gust loads were reached with higher-order nonlinear fiber angle variations when either all plies were optimized or when 2D fiber angle variations were used. Optimization strategies which allowed the fiber angles to vary freely in each ply generally performed better than optimizations based on the rotation of ($0^\circ/\pm 45^\circ/90^\circ$) ply stacks along the span of the wing.

These results demonstrate that tow-steered laminates allow improved designs compared to traditional unidirectional laminates for a 2D wing. The study requires further development to investigate aeroelastic tailoring phenomena of more realistic 3D wing box models using tow-steered composites. Additional mass, structural and aeroelastic tailoring objectives also need to be considered to more accurately assess the potential benefits of using tow-steering for wing structures.

Acknowledgments

The PhD project is funded through a CASE Award granted by the EPSRC and Airbus Operations UK Ltd.

References

- [1] Weisshaar, T. A. "Aeroelastic tailoring of forward swept composite wings," *21st Structures, Structural Dynamics, and Materials Conference*. American Institute of Aeronautics and Astronautics, 1980.
- [2] Shirk, M. H., Hertz, T. J., and Weisshaar, T. A. "Aeroelastic tailoring - Theory, practice, and promise," *Journal of Aircraft* Vol. 23, No. 1, 1986, pp. 6-18
10.2514/3.45260.
- [3] Eastep, F. E., Tischler, V. A., Venkayya, V. B., and Khot, N. S. "Aeroelastic Tailoring of Composite Structures," *Journal of Aircraft* Vol. 36, No. 6, 1999, pp. 1041-1047
10.2514/2.2546.
- [4] Weisshaar, T. A., and Duke, D. K. "Induced Drag Reduction Using Aeroelastic Tailoring with Adaptive Control Surfaces," *Journal of Aircraft* Vol. 43, No. 1, 2006, pp. 157-164
10.2514/1.12040.
- [5] Pettit, C. L., and Grandhi, R. V. "Optimization of a Wing Structure for Gust Response and Aileron Effectiveness," *Journal of Aircraft* Vol. 40, No. 6, 2003, pp. 1185-1191
10.2514/1.10821.
- [6] Kim, T. U., and Hwang, I. H. "Optimal design of composite wing subjected to gust loads," *Computers & Structures* Vol. 83, No. 19-20, 2005, pp. 1546-1554
10.1016/j.compstruc.2005.02.002.
- [7] Arizono, H., and Isogai, K. "Application of Genetic Algorithm for Aeroelastic Tailoring of a Cranked-Arrow Wing," *Journal of Aircraft* Vol. 42, No. 2, 2005, pp. 493-499
10.2514/1.392.
- [8] Kameyama, M., and Fukunaga, H. "Optimum design of composite plate wings for aeroelastic characteristics using lamination parameters," *Computers & Structures* Vol. 85, No. 3-4, 2007, pp. 213-224
10.1016/j.compstruc.2006.08.051.
- [9] Guo, S. "Aeroelastic optimization of an aerobatic aircraft wing structure," *Aerospace Science and Technology* Vol. 11, No. 5, 2007, pp. 396-404
10.1016/j.ast.2007.01.003.
- [10] Guo, S., Li, D., and Liu, Y. "Multi-objective optimization of a composite wing subject to strength and aeroelastic constraints," *Proceedings of the Institution of Mechanical Engineers Part G-Journal of Aerospace Engineering* Vol. 226, No. G9, 2012,
10.1177/0954410011417789.
- [11] Dr. Rubén Del Rosario, M. G. F., Dr. Rich Wahls, Dr. Nateri Madavan. "NASA Subsonic Fixed Wing: Fundamental Technical Challenges," *50th Aerospace Sciences meeting*. AIAA, Nashville, TN, 2012.
- [12] Livne, E. "Future of airplane aeroelasticity," *Journal of Aircraft* Vol. 40, No. 6, 2003, pp. 1066-1092
10.2514/2.7218.
- [13] Hale, R., Moon, R., Lim, K., Schueler, K., and Wiehn, M. "Current Progress on Integrated Design and Analysis Tools for Fiber Steered Composites," *43rd AIAA/ASME/ASCE/AHS/ASC Structures, Structural Dynamics, and Materials Conference*. American Institute of Aeronautics and Astronautics, 2002.
- [14] Weck, O. d., Agte, J., Sobieszczanski-Sobieski, J., Arendsen, P., Morris, A., and Spieck, M. "State-of-the-Art and Future Trends in Multidisciplinary Design Optimization," *48th AIAA/ASME/ASCE/AHS/ASC Structures, Structural Dynamics, and Materials Conference*. American Institute of Aeronautics and Astronautics, 2007.
- [15] Fish, J. C., and Lee, S. W. "Delamination of tapered composite structures," *Engineering Fracture Mechanics* Vol. 34, No. 1, 1989, pp. 43-54
10.1016/0013-7944(89)90241-5.

- [16] Mukherjee, A., and Varughese, B. "Design guidelines for ply drop-off in laminated composite structures," *Composites Part B-Engineering* Vol. 32, No. 2, 2001, pp. 153-164
10.1016/s1359-8368(00)00038-x.
- [17] Soden, P. D., Kaddour, A. S., and Hinton, M. J. "Recommendations for designers and researchers resulting from the world-wide failure exercise," *Composites Science and Technology* Vol. 64, No. 3-4, 2004, pp. 589-604
[http://dx.doi.org/10.1016/S0266-3538\(03\)00228-8](http://dx.doi.org/10.1016/S0266-3538(03)00228-8).
- [18] Ostergaard, M., Ibbotson, A., Roux, O., and Prior, A. "Virtual testing of aircraft structures," *CEAS Aeronautical Journal* Vol. 1, No. 1-4, 2011, pp. 83-103
10.1007/s13272-011-0004-x.
- [19] Davies, G. A. O., and Ankersen, J. "Virtual testing of realistic aerospace composite structures," *Journal of Materials Science* Vol. 43, No. 20, 2008, pp. 6586-6592
10.1007/s10853-008-2695-x.
- [20] Kim, B. C., Potter, K., and Weaver, P. M. "Continuous tow shearing for manufacturing variable angle tow composites," *Composites Part a-Applied Science and Manufacturing* Vol. 43, No. 8, 2012,
10.1016/j.compositesa.2012.02.024.
- [21] Lopes, C. S., Gurdal, Z., and Camanho, P. P. "Variable-stiffness composite panels: Buckling and first-ply failure improvements over straight-fibre laminates," *Computers & Structures* Vol. 86, No. 9, 2008,
10.1016/j.compstruc.2007.04.016.
- [22] Gurdal, Z., Tatting, B. F., and Wu, C. K. "Variable stiffness composite panels: Effects of stiffness variation on the in-plane and buckling response," *Composites Part a-Applied Science and Manufacturing* Vol. 39, No. 5, 2008,
10.1016/j.compositesa.2007.11.015.
- [23] Kuo, S.-Y., and Shiau, L.-C. "Buckling and vibration of composite laminated plates with variable fiber spacing," *Composite Structures* Vol. 90, No. 2, 2009,
10.1016/j.compstruct.2009.02.013.
- [24] Weaver, P., Potter, K., Hazra, K., Saverymuthapulle, M., and Hawthorne, M. "Buckling of Variable Angle Tow Plates: From Concept to Experiment," *50th AIAA/ASME/ASCE/AHS/ASC Structures, Structural Dynamics, and Materials Conference 17th AIAA/ASME/AHS Adaptive Structures Conference 11th AIAA No.* American Institute of Aeronautics and Astronautics, 2009.
- [25] Wu, Z., Weaver, P. M., Raju, G., and Chul Kim, B. "Buckling analysis and optimisation of variable angle tow composite plates," *Thin-Walled Structures* Vol. 60, No. 0, 2012, pp. 163-172
<http://dx.doi.org/10.1016/j.tws.2012.07.008>.
- [26] Lopes, C. S., Gurdal, Z., and Camanho, P. P. "Tailoring for strength of composite steered-fibre panels with cutouts," *Composites Part a-Applied Science and Manufacturing* Vol. 41, No. 12, 2010,
10.1016/j.compositesa.2010.08.011.
- [27] Gliesche, K., Hubner, T., and Orawetz, H. "Application of the tailored fibre placement (TFP) process for a local reinforcement on an "open-hole" tension plate from carbon/epoxy laminates," *Composites Science and Technology* Vol. 63, No. 1, 2003,
10.1016/s0266-3538(02)00178-1.
- [28] Honda, S., and Narita, Y. "Natural frequencies and vibration modes of laminated composite plates reinforced with arbitrary curvilinear fiber shape paths," *Journal of Sound and Vibration* Vol. 331, No. 1, 2012, pp. 180-191
10.1016/j.jsv.2011.08.019.
- [29] Akhavan, H., and Ribeiro, P. "Natural modes of vibration of variable stiffness composite laminates with curvilinear fibers," *Composite Structures* Vol. 93, No. 11, 2011,
10.1016/j.compstruct.2011.04.027.
- [30] Ribeiro, P., and Akhavan, H. "Non-linear vibrations of variable stiffness composite laminated plates," *Composite Structures* Vol. 94, No. 8, 2012,
10.1016/j.compstruct.2012.03.025.
- [31] Abdalla, M. M., Setoodeh, S., and Gurdal, Z. "Design of variable stiffness composite panels for maximum fundamental frequency using lamination parameters," *Composite Structures* Vol. 81, No. 2, 2007,

10.1016/j.compstruct.2006.08.018.

[32] Thuwis, G., Abdalla, M., and Gürdal, Z. "Optimization of a variable-stiffness skin for morphing high-lift devices," *Smart materials and structures* Vol. 19, No. 12, 2010, p. 124010

[33] Haddadpour, H., and Zamani, Z. "Curvilinear fiber optimization tools for aeroelastic design of composite wings," *Journal of Fluids and Structures* Vol. 33, 2012,
10.1016/j.jfluidstructs.2012.05.008.

[34] Stodieck, O., Cooper, J. E., Weaver, P. M., and Kealy, P. "Improved Aeroelastic Tailoring Using Tow-Steered Composites," *Composite Structures* Vol. 106, 2013, pp. 703-715
10.1016/j.compstruct.2013.07.023.

[35] Wu, Z., Weaver, P. M., and Raju, G. "Postbuckling optimisation of variable angle tow composite plates," *Composite Structures* Vol. 103, No. 0, 2013, pp. 34-42
<http://dx.doi.org/10.1016/j.compstruct.2013.03.004>.

[36] Ghiasi, H., Pasini, D., and Lessard, L. "Optimum stacking sequence design of composite materials Part I: Constant stiffness design," *Composite Structures* Vol. 90, No. 1, 2009, pp. 1-11
10.1016/j.compstruct.2009.01.006.

[37] Ghiasi, H., Fayazbakhsh, K., Pasini, D., and Lessard, L. "Optimum stacking sequence design of composite materials Part II: Variable stiffness design," *Composite Structures* Vol. 93, No. 1, 2010,
10.1016/j.compstruct.2010.06.001.

[38] Irisarri, F.-X., Abdalla, M. M., and Gurdal, Z. "Improved Shepard's Method for the Optimization of Composite Structures," *Aiaa Journal* Vol. 49, No. 12, 2011,
10.2514/1.j051109.

[39] Weisshaar, T. A., and Foist, B. L. "Vibration tailoring of advanced composite lifting surfaces," *Journal of Aircraft* Vol. 22, No. 2, 1985, pp. 141-147
10.2514/3.45098.

[40] Braaten, E., and Weller, G. "Improved Low-Discrepancy Sequence for Multidimensional Quasi-Monte Carlo Integration," *Journal of Computational Physics* Vol. 33, No. 2, 1979, pp. 249-258
Doi 10.1016/0021-9991(79)90019-6.

[41] Wu, Z., Raju, G., and Weaver, P. "Comparison of Variational, Differential Quadrature, and Approximate Closed-Form Solution Methods for Buckling of Highly Flexurally Anisotropic Laminates," *Journal of Engineering Mechanics* Vol. 139, No. 8, 2013, pp. 1073-1083
doi:10.1061/(ASCE)EM.1943-7889.0000468.

[42] Hancock, G. J. *An Introduction to the Flight Dynamics of Rigid Aeroplanes*: Ellis Horwood, New York, 1995.

[43] "Matlab R2012a Global Optimization Toolbox." The MathWorks, Inc., 2012.

[44] R. Tatham, B. A., A.F.R.Ae.S. "Shear Centre, Flexural Centre and Flexural Axis: An Attempt to Clear up Current Confusion and Provide Definitions Differentiating Between the Three Terms," *Aircraft Engineering and Aerospace Technology* Vol. 23, No. 7, 1951, pp. 209 - 210
10.1108/eb032058.

[45] EASA. "CS/AMC 25.341," *CS-25/14*. 2013.

[46] Deb, K. *Multi-objective optimization using evolutionary algorithms*. Chichester ; New York: John Wiley & Sons, 2001.